Coupled Dynamic–Thermodynamic Forcings during Tropical Cyclogenesis. Part I: Diagnostic Framework

BRIAN H. TANG

Department of Atmospheric and Environmental Sciences, University at Albany, State University of New York, Albany, New York

(Manuscript received 16 February 2017, in final form 25 April 2017)

ABSTRACT

A diagnostic framework to investigate the role of processes around and during tropical cyclogenesis is presented. The key framework metric is the ratio of bulk differences of moist entropy over differences of angular momentum between an inner and outer region of a tropical disturbance or cyclone. This ratio is hypothesized to decrease and become negative as both the high-entropy core and low-level vortex in the inner region amplify during tropical cyclogenesis. The time tendency of this ratio can be split into two forcings: a moist entropy forcing and an angular momentum forcing. Each forcing can be further divided into components comprising differences in net advective fluxes and nonadvective boundary fluxes of moist entropy or angular momentum between each region. The framework provides a comprehensive way to compare the relative importance of processes leading to tropical cyclogenesis in a tractable, consistent manner. Suggestions on how to apply the framework to numerical model output are given.

1. Introduction

Tropical cyclogenesis is a multiscale process with a strong coupling between the dynamics of the circulation and the thermodynamics of moist convection (Simpson et al. 1997). While numerical modeling of tropical cyclogenesis has become increasingly sophisticated and skillful from an operational perspective (Halperin et al. 2013), there remain a number of open questions and hypotheses concerning the relevant or dominant physical processes during tropical cyclogenesis. One fundamental question is how the low-level vortex forms and amplifies.

Early perspectives focused on the spinup of the system-scale, low-level vortex from an axisymmetric point of view. Convective heating near the disturbance center results in a thermally direct circulation that has a radial inflow branch below the level of maximum heating (Charney and Eliassen 1964; Willoughby 1979; Shapiro and Willoughby 1982). More recently, Smith et al. (2009) noted that unbalanced forces are important for the development of the radial inflow within the boundary layer. Above the boundary layer, where friction is small, conservation of angular momentum results in an acceleration of the tangential winds as parcels travel toward smaller radius. Within the boundary layer, the convergence of the angular momentum flux exceeds frictional torques to spin up the inner circulation.

In addition to the axisymmetric point of view, cyclonic absolute vorticity asymmetries can merge and axisymmetrize, resulting in an upscale transfer of energy and vortex spinup (Montgomery and Enagonio 1998; Moller and Montgomery 2000; Enagonio and Montgomery 2001). The source of these asymmetries is rotating deep convection, or vortical hot towers (VHTs) (Davis and Bosart 2001; Hendricks et al. 2004; Montgomery et al. 2006; Kilroy and Smith 2013), and cumulus congestus (Wang 2014), primarily through stretching of background absolute vorticity. The concentration of cyclonic absolute vorticity in a circular region must correspond to an increase in the angular momentum at the boundary of the circular region, so the vorticity and angular momentum perspectives are dynamically intertwined.

Purely dynamical perspectives of tropical cyclogenesis are useful for understanding the spinup of the circulation but cannot provide a complete paradigm for tropical cyclogenesis because of the importance of thermodynamics, including surface enthalpy fluxes, moistening, and latent heat release in moist convection. Surface

Corresponding author: Brian H. Tang, btang@albany.edu

DOI: 10.1175/JAS-D-17-0048.1

enthalpy fluxes provide the energy needed for the growth of a finite-amplitude disturbance in idealized, axisymmetric models (Ooyama 1969; Emanuel 1989) and fuel the local buoyancy of asymmetric convection in 3D models (Montgomery et al. 2009).

Moist convection also moistens the free troposphere. Nolan (2007) found that the formation of the low-level vortex in numerical simulations generally occurs after the relative humidity exceeds 80% through a deep column within 150 km of the center. A number of observational studies have also found that a deep-tropospheric layer of near saturation precedes tropical cyclogenesis (Bister and Emanuel 1997; Raymond et al. 1998, 2011; Davis and Ahijevych 2012; Wang 2012; Komaromi 2013; Zawislak and Zipser 2014). The high column relative humidity acts to increase the precipitation efficiency in a recirculating ''pouch'' region (Dunkerton et al. 2009; Wang 2012). High-precipitation-efficiency convection increases the moist entropy through a deep column (Emanuel 1989). Lifting at the edge of convectively produced cold pools triggers new deep convection and may be beneficial for tropical cyclogenesis (Montgomery et al. 2006; Davis 2015).

Latent heating in deep, high-precipitation convection builds the warm-core structure at upper levels of the interior region of the disturbance (Zhang and Zhu 2012). Additionally, subsidence warming beneath the melting layer within mesoscale convective systems produces warm anomalies lower in the troposphere (Kerns and Chen 2015). Warming at mid- to upper levels of the troposphere may produce hydrostatic pressure falls at the surface that slowly spin up the system-scale vortex.

There are three components that must be linked together: the moistening that occurs well ahead of tropical cyclogenesis, the growth of the interior warm core, and the spinup of the low-level vortex. A holistic, diagnostic framework must consider all these components and their interactions, which can be challenging to accomplish in a tractable manner.

As a starting point, one can link the vortex and (virtual) temperature structure components together through thermal-wind or nonlinear balance, which states that a balanced vortex with vertical structure must coincide with horizontal gradients in virtual or density potential temperature (Emanuel 1994). The question is whether thermal-wind balance serves as a good approximation of the azimuthally averaged, mesoscale vortex on time scales longer than convective time scales, $O(1)$ h, during tropical cyclogenesis. Ooyama (1982) noted the importance of the reduction in the Rossby radius of deformation during tropical cyclogenesis, bringing the quasi-balanced flow regime down to the mesoscale. Adjustment from an initially unbalanced perturbation to quasi-balanced flow occurs on time scales of about half a day—a characteristic local inertial period for a weak vortex of tropical disturbance strength.

More recently, field campaign observations support the hypothesis that the azimuthally averaged, mesoscale vortex is close to a balanced state. Raymond (2012) and Raymond et al. (2014) found a close balance between the pre-Nuri (2008) disturbance vortex and virtual potential temperature anomalies. Positive virtual potential temperature anomalies existed above the height of the maximum azimuthal wind at midlevels, while negative virtual potential temperature anomalies existed below the height of the maximum azimuthal wind. These anomalies achieved a maximum amplitude near the center of the pre-Nuri disturbance. The negative virtual potential temperature anomalies in the lower troposphere must be eradicated in order for tropical cyclogenesis to occur (Bister and Emanuel 1997).

While thermal-wind balance is a useful starting point and will serve to motivate the framework that will be introduced, there are several limitations. The first limitation is that thermal-wind balance does not have any time dependence and therefore cannot give insight into forcing mechanisms and the subsequent response toward a balanced state, the response being a secondary circulation (Shapiro and Willoughby 1982). The secondary circulation can take on different structures depending on latent heating vertical profiles associated with a spectrum of cloud and precipitation modes. For instance, Montgomery et al. (2006) found the heating profile associated with VHTs in their simulations produced two radial inflow branches—one between 0 and 2 km and one between 6 and 9 km—and a dominant outflow branch between 9 and 14 km. Shallow convection, such as cumulus congestus, has an outflow branch where detrainment occurs, between 2 and 8 km (Wang 2014). Stratiform precipitation typically has midlevel inflow and outflow at both upper and lower levels (Houze 1997).

The second limitation is that water vapor is a small proportion of horizontal density perturbations that constitute thermal-wind balance (Bryan and Rotunno 2009), and water vapor plays a limited role in directly determining the balanced vortex structure. Nonetheless, a meso-beta-scale region of near saturation appears necessary in order for the tropical cyclone protovortex to develop (Wang 2014), so water vapor does indirectly determine the vortex structure. Emanuel (1997) proved that the convectively induced subsidence cannot alone raise the average saturation entropy (temperature) in subsiding regions to a value greater than the saturation entropy (temperature) in convection. Therefore, greater

water vapor in the subcloud layer and in the convecting environment aloft, which minimizes entrainment of relatively low-entropy air, has more potential to increase the vertically averaged temperature and build the warm core in both convecting and adjacent subsiding regions (Kerns and Chen 2015).

It will be advantageous to use the moist entropy as a linchpin between temperature and moisture, as the two are inextricably linked in convective processes. Zawislak and Zipser (2014) composited dropsondes within 300 km of the center of 12 developing disturbances. Positive moist entropy anomalies exist through most of the free troposphere several days prior to genesis and expand in depth and magnitude as genesis approaches. At the same time, neutral to negative moist entropy anomalies exist at low levels but become positive after genesis occurs. Cold anomalies at low levels are responsible for the negative moist entropy anomalies (Komaromi 2013), but moist anomalies compensate somewhat.

The third limitation is the boundary layer imposes its own imbalance and agradient response due to friction that modifies the radial inflow structure (Smith et al. 2009), partially controlling the radial distribution of angular momentum and moist entropy within the boundary layer. Convection can then communicate this distribution to the free troposphere (Raymond 1995). Meanwhile, there is a constant adjustment occurring in the free troposphere toward a balanced state, but as observations show, is always near balance when looking at appropriate spatial and time scales. In other words, while the boundary layer itself is not in balance, the distribution of moist entropy and angular momentum within the boundary layer plays a role in setting the balanced state over the free troposphere.

The goal is to create a diagnostic framework that is motivated by thermal-wind balance but also allows for time dependence and imbalance, and incorporates the critical role of water vapor in order to holistically investigate coupled dynamic–thermodynamic forcings during tropical cyclogenesis. Section 2 presents the framework, section 3 suggests potential applications of the framework, and section 4 concludes with a summary of the framework.

2. Framework

The thermodynamic state variable is the moist entropy s (Tang and Emanuel 2012):

$$s = \underbrace{c_{pd}\log\Theta}_{s_\Theta} + \underbrace{\frac{L_v q}{T_L}}_{s_q} - R_d \log p_o, \tag{1}$$

where c_{pd} is the specific heat at constant pressure of dry air, Θ is the potential temperature, L_v is the latent heat of vaporization, q is the water vapor mixing ratio, T_L is the saturation temperature, R_d is the gas constant for dry air, and p_o is the reference pressure. In lieu of the moist entropy, one can also use any variable that is quasi conserved in moist adiabatic processes, such as the ice–liquid potential temperature or the moist static energy. The choice here is motivated by the use of (1) in a numerical model that the framework will be applied to in Tang (2017, hereafter Part II). Since it may be useful to examine the effects of warming and moistening separately, the first two terms on the rhs of (1) are defined as s_Θ and s_q, respectively.

The dynamic state variable is the absolute angular momentum:

$$M = rv + \frac{fr^2}{2}, \tag{2}$$

where r is the radius, v is the tangential wind, and f is the Coriolis parameter.

It will be useful to consider variations in moist entropy with respect to angular momentum (Schubert and Hack 1983). Emanuel (1997) used a thermal-wind expression in angular momentum coordinates to investigate axisymmetric, slantwise frontogenesis in tropical cyclones. Frontogenesis occurs as moist entropy surfaces compress relative to angular momentum surfaces with a concomitant increase in the tangential winds of the low-level vortex. A goal of this study is to create a metric that is based off the proposition that gradients of moist entropy with respect to angular momentum are relevant to the development of the low-level vortex.

We approximate the gradient of moist entropy with respect to angular momentum through differences in each variable across two regions. Figure 1 illustrates the two regions. The inner cylindrical region has a radius of r_i and the outer annular region extends from r_i to r_o. Both regions have a height of z_t. For simplicity, it is assumed the center of the tropical disturbance and regions is stationary but can be generalized to be in the comoving frame of reference with the disturbance. We will recommend appropriate choices for r_i, r_o, and z_t in the next section but are purposely vague here for generality.

For a given region, the averaging operator is

$$[x] \equiv \frac{\iiint \rho x \, dV}{\iiint \rho \, dV}, \quad x \in \{M, s\}, \tag{3}$$

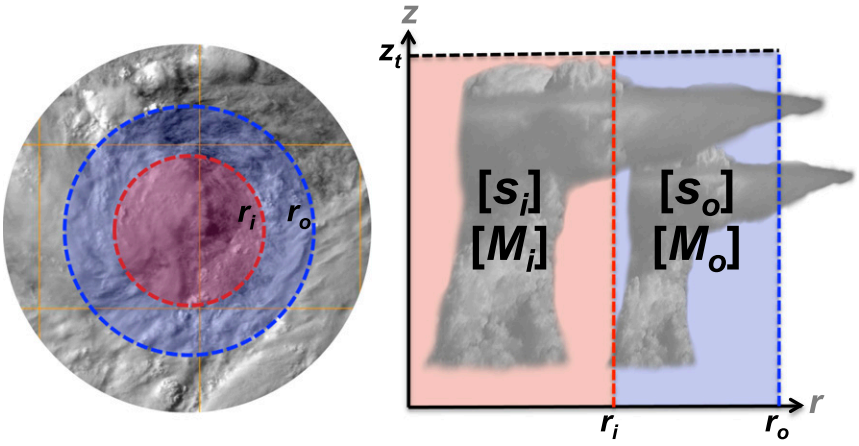

FIG. 1. (left) A planar view of a hypothetical tropical disturbance with inner (red) and outer (blue) regions and (right) a radius–height illustration of averages of moist entropy and angular momentum in both regions. This and subsequent figures are not to scale.

where the square brackets denote the averaging operator and ρ is the dry density. Applying (3) to both the moist entropy and angular momentum in each region and then taking the difference results in bulk differences between the inner and outer regions:

$$\Delta s = [s_i] - [s_o] \quad \text{and} \tag{4}$$

$$\Delta M = [M_i] - [M_o]. \tag{5}$$

The nondimensional bulk gradient of moist entropy with respect to angular momentum χ can then be expressed as

$$\chi = \alpha \frac{\Delta s}{\Delta M}, \tag{6}$$

and α is a constant given by

$$\alpha = \left| \frac{\Delta M_{\text{ref}}}{\Delta s_{\text{ref}}} \right|, \tag{7}$$

where $\Delta M_{\text{ref}} = [M_{p,i}] - [M_{p,o}]$ is a reference bulk difference of planetary angular momentum ($M_p = 0.5fr^2$) between the inner and outer regions. The choice of ΔM_{ref} serves to approximately normalize ΔM regardless of the choice of regions. The reference bulk difference of moist entropy Δs_{ref} is set to $1\ \text{J kg}^{-1}\ \text{K}^{-1}$, motivated by a typical order of magnitude for observed tropical disturbances (Zawislak and Zipser 2014).

Both the distribution of moist entropy and angular momentum in each region affects the magnitude of χ. For an inertially stable vortex, ΔM must always be negative. On the other hand, Δs can be either positive or negative and thus controls the sign of χ.

Figure 2 conceptualizes how χ may behave for tropical disturbances undergoing genesis. Figures 2a and 2b illustrate archetype tropical disturbances with vortices that reach a maximum amplitude at midlevels and low levels, respectively. Nicholls and Montgomery (2013) found that tropical disturbances undergoing genesis in numerical simulations vary in a continuum between the two archetypes.

A midlevel vortex is commonly observed in both observations and models during the pregenesis phase of tropical disturbances (Bister and Emanuel 1997; Houze 1997, 2010). The angular momentum contours bow inward as a result of midlevel inflow associated with stratiform precipitation. A midlevel vortex is associated with negative (positive) horizontal perturbations of s_Θ below (above) the level of maximum tangential wind and angular momentum (Raymond 2012; Raymond et al. 2014). These perturbations decay away from the center.

Low-level convergence and stretching of positive absolute vorticity contribute to the development of the low-level vortex (Hendricks et al. 2004). The angular momentum contours bow inward as a result of low-level inflow associated with convective precipitation. A low-level vortex is associated with positive horizontal perturbations of s_Θ above the level of maximum tangential wind and angular momentum near the top of the boundary layer. Within the boundary layer, negative horizontal perturbations s_Θ may still remain owing to convective cold pools (Davis 2015).

Meanwhile in both Figs. 2a and 2b, moistening due to the accumulated effects of convection results in positive horizontal perturbations of s_q that maximize

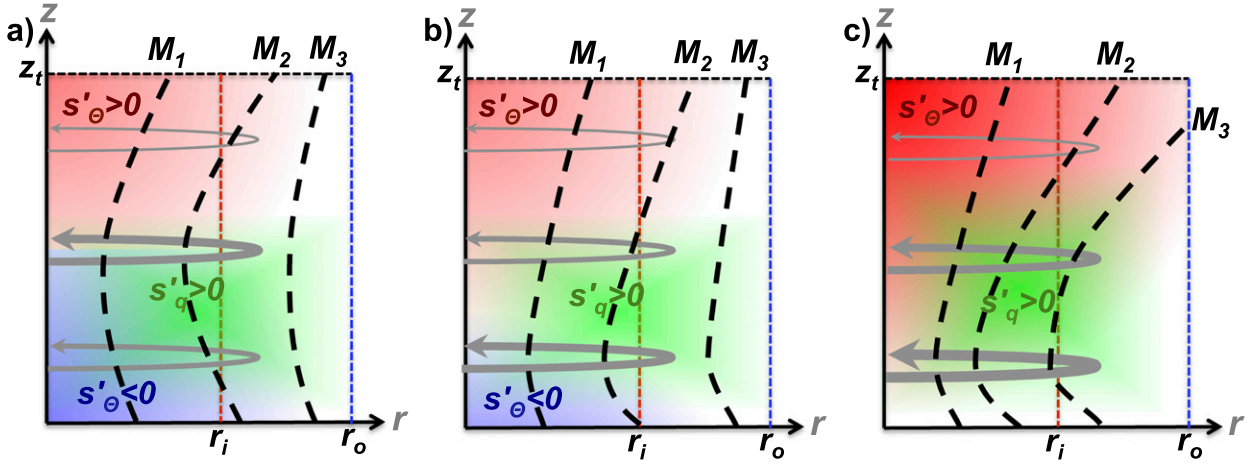

FIG. 2. Conceptual illustration of azimuthally averaged horizontal moist entropy perturbations due to thermal perturbations (red and blue shading) and moisture perturbations (green shading), and angular momentum (dashed black lines) for (a) a tropical disturbance with a maximum vortex amplitude at midlevels, (b) a tropical disturbance with a maximum vortex amplitude at low levels, and (c) a postgenesis tropical cyclone.

at midlevels. These perturbations exist a couple of days before genesis (Wang 2012; Zawislak and Zipser 2014).

The sign of χ for the scenarios in Figs. 2a and 2b is ambiguous. There are offsetting effects between negative s_Θ anomalies and positive s_q anomalies in the lower and/or middle troposphere. Dropsonde observations in developing tropical disturbances suggest the positive s_q anomalies dominate, yielding positive horizontal perturbations of moist entropy at midlevels (Zawislak and Zipser 2014). Additionally, there is cancellation between the negative and positive moist entropy anomalies in each region, so the sign of χ depends on the depth and magnitude of these anomalies in each region and on the choice of the regions themselves. Nonetheless, given the cancellation of opposite signed anomalies and the small magnitude of the moist entropy anomalies in observed tropical disturbances, we hypothesize that χ is small ($|\chi| \lesssim 1$) in the pregenesis phase.

The defining characteristic of tropical cyclogenesis is the formation of a low-level vortex of sufficient longevity and strength (Nolan 2007) or, more specifically, a meso-beta-scale protovortex within the meso-alpha-scale circulation (Dunkerton et al. 2009; Wang 2012). The positive moist entropy anomalies increase in magnitude and depth, owing to both s_Θ and s_q, and the angular momentum surfaces move inward at low levels and flare outward at upper levels (Fig. 2c). As a result, there is no longer ambiguity in the sign of χ after genesis—that is, χ must be negative because Δs is positive—while ΔM remains negative. From the two tropical disturbance archetypes in Figs. 2a and 2b to the postgenesis tropical cyclone in Fig. 2c, there has been a decrease in χ, suggesting that a negative time tendency in χ around the time of tropical cyclogenesis is necessary.

The time tendency of χ can be split into two terms:

$$\frac{\partial \chi}{\partial t} = \underbrace{\frac{\alpha}{\Delta M}\frac{\partial}{\partial t}(\Delta s)}_{\sigma_s} - \underbrace{\frac{\alpha \Delta s}{(\Delta M)^2}\frac{\partial}{\partial t}(\Delta M)}_{\sigma_M} . \tag{8}$$

The first term on the rhs is defined as the moist entropy forcing σ_s, and the second term is defined as the angular momentum forcing σ_M. Note that the time tendencies are scaled by factors involving the bulk differences themselves, making the terms in (8) strongly nonlinear.

Using (3) and (4), σ_s can be expanded:

$$\sigma_s = \frac{\alpha}{\Delta M}\frac{\partial}{\partial t}\left(\frac{\int_0^{z_t}\int_0^{2\pi}\int_0^{r_i} \rho s r\, dr\, d\theta\, dz}{\int_0^{z_t}\int_0^{2\pi}\int_0^{r_i} \rho r\, dr\, d\theta\, dz} - \frac{\int_0^{z_t}\int_0^{2\pi}\int_{r_i}^{r_o} \rho s r\, dr\, d\theta\, dz}{\int_0^{z_t}\int_0^{2\pi}\int_{r_i}^{r_o} \rho r\, dr\, d\theta\, dz} \right) . \tag{9}$$

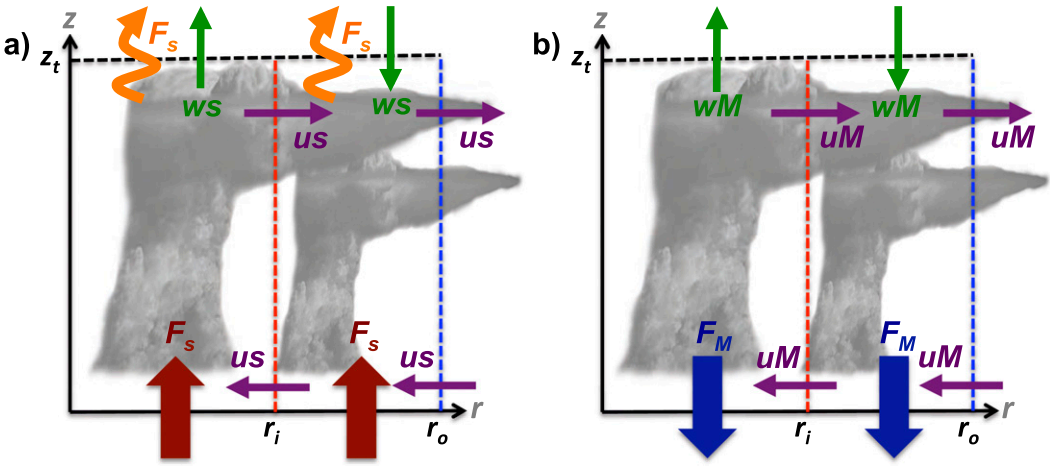

FIG. 3. (a) Moist entropy budget and (b) angular momentum budget in the inner and outer regions. Purple arrows are radial advective fluxes through r_i and r_o, green arrows are vertical advective fluxes through z_t, orange arrows are radiative fluxes of moist entropy at z_t, red arrows are surface fluxes of moist entropy, and blue arrows are surface fluxes of angular momentum.

The denominators of the terms inside the parentheses are the masses of each respective region, which will generally vary with time for a fixed region. Instead, the mass in each region can be fixed in time by allowing r_i and r_o to be time-evolving boundaries, such that

$$m_i = \int_0^{z_t}\int_0^{2\pi}\int_0^{r_i(t)} \rho r\, dr\, d\theta\, dz \quad \text{and} \tag{10}$$

$$m_o = \int_0^{z_t}\int_0^{2\pi}\int_{r_i(t)}^{r_o(t)} \rho r\, dr\, d\theta\, dz\,. \tag{11}$$

As a result, m_i is fixed by the initial choice of r_i, and m_o is fixed by the initial choice of r_i and r_o. For all time, r_i and r_o are then determined such that (10) and (11) hold. Using (10) and (11) in (9) and bringing the time derivative inside the integral,

$$\sigma_s = \frac{\alpha}{\Delta M}\left\{\frac{1}{m_i}\int_0^{z_t}\int_0^{2\pi}\left[\int_0^{r_i}\frac{\partial}{\partial t}(\rho s)r\, dr + (\rho s r)|_{r_i}\dot{r}_i\right] d\theta\, dz \right.$$
$$\left. -\frac{1}{m_o}\int_0^{z_t}\int_0^{2\pi}\left[\int_{r_i}^{r_o}\frac{\partial}{\partial t}(\rho s)r\, dr + (\rho s r)|_{r_o}\dot{r}_o - (\rho s r)|_{r_i}\dot{r}_i\right] d\theta\, dz\right\}, \tag{12}$$

where $\dot{r}_i$ and $\dot{r}_o$ are the time rates of change of r_i and r_o, respectively. The moist entropy equation is

$$\frac{\partial}{\partial t}(\rho s) = -\nabla\cdot(\mathbf{u}\rho s) - \nabla\cdot\mathbf{F}_s, \tag{13}$$

where $\mathbf{u}$ is the wind velocity and $\mathbf{F}_s$ is nonadvective boundary fluxes of moist entropy. Small, irreversible sources of moist entropy, such as rain evaporating into subsaturated air, are ignored. Upon substituting (13) into (12) and using the divergence theorem,

$$\sigma_s = \frac{\alpha}{\Delta M}\left[-\left(\frac{1}{m_i}+\frac{1}{m_o}\right)\int_0^{z_t}\int_0^{2\pi}(u-\dot{r}_i)\rho s r|_{r_i}\, d\theta\, dz \right.$$
$$+\frac{1}{m_o}\int_0^{z_t}\int_0^{2\pi}(u-\dot{r}_o)\rho s r|_{r_o}\, d\theta\, dz - \frac{1}{m_i}\int_0^{2\pi}\int_0^{r_i} w\rho s|_{z_t} r\, dr\, d\theta$$
$$\left. +\frac{1}{m_o}\int_0^{2\pi}\int_{r_i}^{r_o} w\rho s|_{z_t} r\, dr\, d\theta + \frac{1}{m_i}\int_0^{2\pi}\int_0^{r_i} F_s^{\text{net}} r\, dr\, d\theta - \frac{1}{m_o}\int_0^{2\pi}\int_{r_i}^{r_o} F_s^{\text{net}} r\, dr\, d\theta\right], \tag{14}$$

where u is the radial wind, w is the vertical wind, and $F_s^{\text{net}} = F_s(z=0) - F_s(z_t)$ is the net column nonadvective flux of moist entropy. Figure 3a shows the components of the moist entropy budget in each region that form the terms in (14). Since $\Delta M < 0$, any term that is positive inside the brackets contributes to reducing χ, tending toward a (stronger) warm moist-core structure and low-level vortex.

The first two terms on the rhs of (14) involve radial fluxes of moist entropy through the lateral boundaries of each region. Note the radial velocity is relative to the movement of r_i and r_o, which both generally move outward during tropical cyclogenesis as surface pressures fall within each region. The movement of both r_i and r_o is slow, less than $1\,\text{cm}\,\text{s}^{-1}$, and is generally much less than typical radial flows in the inflow and outflow layers. The third and fourth terms on the rhs of (14) involve vertical fluxes of moist entropy through the top of each region. The vertical flux is assumed to vanish at the bottom ($z = 0$). The first four terms combined represent the advective flux component of the moist entropy forcing.

Differences in the net advective flux into each region change Δs. For example, a net advective flux of moist entropy into the inner region and a net advective flux of moist entropy out of the outer region increase Δs. These terms may be interpreted in terms of the gross moist stability (GMS) (Neelin and Held 1987; Raymond et al. 2007, 2009), defined generically as the vertically integrated horizontal divergence of the moist entropy flux divided by some measure of the convective strength or moisture flux divergence. Unlike past derivations of the GMS, the vertical velocity in this framework is not assumed to vanish at the top boundary.

The response of convection to different GMS values has been studied in TCs. A smaller normalized GMS corresponds to convection with bottom-heavy vertical mass flux profiles and more rapid spinup of the low-level vortex (Raymond and Sessions 2007; Raymond et al. 2014). Here, differences in GMS between the two regions may be important. If the sum of the first four terms on the rhs of (14) is negative, it is equivalent to a positive radial gradient of GMS in a bulk sense. The necessity of such a gradient for tropical cyclogenesis was speculated by Raymond et al. (2007).

The final two terms on the rhs of (14) involve net column moist entropy fluxes due to radiation and surface fluxes in each region. A greater net column moist entropy flux in the inner region compared to the outer region increases Δs. This increase in Δs may manifest in two ways: larger surface enthalpy fluxes and/or smaller amounts of radiative cooling in the inner region compared to the outer region. The former may be accomplished if the surface winds in the inner region amplify at a greater rate than the outer region.

All of the terms are scaled by ΔM^{-1}. As a result, decreasing the magnitude of ΔM yields a larger moist entropy forcing for the same magnitude of the sum of the terms within brackets in (14). The term ΔM has a smaller magnitude for a vortex that has a sharply peaked tangential wind profile with a radius of maximum tangential wind in the inner region versus a vortex that has a broad tangential wind profile.

The expansion and derivation for σ_M follows almost identically as σ_s. Using the angular momentum equation,

$$\frac{\partial}{\partial t}(\rho M) = -\nabla \cdot (\mathbf{u}\rho M) - \frac{dF_M}{dz}, \tag{15}$$

where F_M is boundary fluxes of angular momentum due to frictional torques, σ_M can be expressed as

$$\begin{aligned}\sigma_M = \frac{\alpha \Delta s}{(\Delta M)^2}\Bigg[&\left(\frac{1}{m_i}+\frac{1}{m_o}\right)\int_0^{z_t}\int_0^{2\pi}(u-\dot{r}_i)\rho M r|_{r_i}\,d\theta\,dz \\ &-\frac{1}{m_o}\int_0^{z_t}\int_0^{2\pi}(u-\dot{r}_o)\rho M r|_{r_o}\,d\theta\,dz+\frac{1}{m_i}\int_0^{2\pi}\int_0^{r_i} w\rho M|_{z_t} r\,dr\,d\theta \\ &-\frac{1}{m_o}\int_0^{2\pi}\int_{r_i}^{r_o} w\rho M|_{z_t} r\,dr\,d\theta-\frac{1}{m_i}\int_0^{2\pi}\int_0^{r_i} F_M|_{z=0} r\,dr\,d\theta+\frac{1}{m_o}\int_0^{2\pi}\int_{r_i}^{r_o} F_M|_{z=0} r\,dr\,d\theta\Bigg].\end{aligned} \tag{16}$$

Figure 3b shows the components of the angular momentum budget in each region that form the terms in (16). The interpretation of the terms is similar to those in the moist entropy forcing but is made ambiguous owing to the dependence on the sign of Δs. For $\Delta s > 0$, any term that is negative inside the brackets contributes to decreasing χ. The first four terms combined represent the advective flux component of the angular momentum forcing. If the net flux of angular momentum into the inner region is larger than the outer region, ΔM becomes less negative. Hence, any process that can concentrate angular momentum in the inner region faster than the

outer region, like low-level convergence associated with convection or system-scale inflow, may contribute to decreasing χ. The final two terms on the rhs of (16) involve surface angular momentum fluxes. If the surface angular momentum flux is more negative in the outer region compared to the inner region, ΔM also becomes less negative.

All of the terms are scaled by $\Delta s(\Delta M)^{-2}$, so increasing the magnitude of Δs and decreasing the magnitude of ΔM contribute to a larger angular momentum forcing. Therefore, a tendency to preferentially spin up the vortex and deepen or strengthen the high-entropy core in the inner region amplifies the bracketed terms in (16).

In summary, (8), (14), and (16) represent a diagnostic framework for studying tropical cyclogenesis processes as a coupled dynamic–thermodynamic system. We now summarize the key assumptions. The first assumption is the azimuthally averaged vortex above the boundary layer is in approximate thermal-wind balance (Raymond 2012). As such, the framework should be applied over time scales at and longer than half a day and spatial scales within the meso-beta scale (20–200 km), where balance is more likely to apply. Irreversible sources of moist entropy in the interior of the regions are ignored. Although motivated by balanced dynamics to form χ, the framework does not assume strict balanced dynamics, axisymmetry, or a steady state. Clearly, the secondary circulation and processes within the boundary layer may be important, particularly the role of radial advective fluxes and surface fluxes.

3. Potential applications

In Part II, we apply the diagnostic framework to a set of axisymmetric tropical cyclogenesis experiments to assess the relative roles of the moist entropy and angular momentum forcing components. For generality, we give some guidelines and caveats that will allow the diagnostic framework to be applied to a variety of models.

The framework requires specification of initial values of r_i, r_o, and z_t. Since the key structural feature is the emergence of the meso-beta-scale low-level protovortex, it is important to choose the inner and outer regions to appropriately capture its development. A good starting point is to choose r_i to be the approximate location at which the low-level radius of maximum wind of the protovortex emerges in order to understand processes around this critical location. Then, r_o is chosen such that the distance between r_o and r_i falls within the meso-beta scale. Setting z_t just above the initial height of the tropopause allows for the full secondary circulation to be captured.

The choice of region boundaries should be guided by the a posteriori output from a tropical cyclogenesis simulation. There are a couple caveats to keep in mind. Having too large of an outer or inner region would render the framework suboptimal, as it would lack resolution of processes occurring around the developing protovortex. Notwithstanding, larger regions may be chosen to investigate the meso-alpha-scale characteristics of spinup. Having too small of an outer or inner region could violate the assumption that the regions exist in a quasi-balanced state and potentially lead to increased unbalanced noise.

A vortex center must be identified in order to interpolate the fields to cylindrical coordinates, and the center movement calculated so that horizontal velocities are in a frame of reference following the vortex center. Determining the center of a tropical disturbance is nontrivial. Nguyen et al. (2014) discuss center identification techniques and found that the pressure centroid method produces a smooth track and is insensitive to changes in horizontal grid resolution. A smooth track is preferable because it minimizes large shifts in center movement that would create unrepresentative advective fluxes in the comoving frame of reference.

There is typically large cancellation in horizontal and vertical advective fluxes of moist entropy (Raymond et al. 2009), and it is necessary to have high-time-resolution output in order to calculate the relatively small net advective flux. One must be careful in assuming the vertical advective fluxes vanish at z_t, even if z_t is set above the tropopause. Although vertical velocities may be small, the moist entropy or other similar quantities is large.

Last, some time filtering of each of moist entropy and angular momentum forcing components is generally needed to filter out frequencies with periods less than half a day to decrease unbalanced noise. Such a filter may be a simple time average to more sophisticated spectral filters.

Provided the above criteria are satisfied, the framework may then be used to assess the behavior of χ before, during, and after genesis (provided a suitable definition of genesis in a model), the relative roles of the moist entropy and angular momentum forcings in determining changes in χ, which components of the forcings dominate, and how these components change with time. The framework provides a comprehensive and tractable way to evaluate and compare processes potentially important for tropical cyclogenesis in a consistent manner.

4. Conclusions

Tropical cyclogenesis involves dynamical and thermodynamical processes that are strongly coupled to one

another. A simple way to express this coupling is through a ratio of bulk differences of moist entropy over bulk differences of angular momentum between inner and outer regions. This ratio χ is motivated by prior studies that have shown gradients of moist entropy with respect to angular momentum are relevant to the development of a tropical cyclone. Above the boundary layer, observational studies of developing tropical disturbances have shown that the vortex is near thermal-wind balance. We hypothesize that a negative time tendency in χ around the time of tropical cyclogenesis is necessary, a reflection of the strengthening and deepening high-entropy core and the inward advection of angular momentum that spins up a coherent low-level vortex.

We hypothesize that a decrease in χ is a metric that tropical cyclogenesis is occurring. However, the underlying processes that control the tendencies in moist entropy and angular momentum in each region can be dissected further, yielding a diagnostic framework for comparing processes before, during, and after tropical cyclogenesis. These processes include advective fluxes through the lateral and top boundaries of each region, surface fluxes of moist entropy, frictional torques of angular momentum, and net radiative fluxes.

Although the formulation of χ is motivated by thermal-wind balance, the framework has relatively few assumptions. The assumptions are the azimuthal-average vortex above the boundary layer is nearly in balance on time scales greater than 12 h and spatial scales at and larger than the meso-beta scale, and internal, irreversible sources of moist entropy can be ignored. Strict balanced dynamics, axisymmetry, steady state, and assumptions about the structure of the boundary layer are not required.

The framework can address a number of possible questions. First, how does χ evolve in numerical simulations of tropical cyclogenesis, and is there a characteristic feature in the evolution of χ that signifies genesis is occurring? If so, how does the moist entropy or angular momentum forcing dictate the evolution of χ before and during genesis? Second, are there differences in the net advective flux of moist entropy between the regions that imply the existence of a radial gradient of GMS, and if so, how does this gradient evolve around genesis? Third, does a radial gradient of the GMS or differential surface fluxes between the regions matter more to amplifying the high-entropy core? These questions will be addressed in Part II.

Acknowledgments. Will Komaromi and two anonymous reviewers helped improve the manuscript. The University at Albany Faculty Research Award Program Award 64949 supported a portion of this work.

REFERENCES

Bister, M., and K. A. Emanuel, 1997: The genesis of Hurricane Guillermo: TEXMEX analyses and a modeling study. *Mon. Wea. Rev.*, **125**, 2662–2682, doi:10.1175/1520-0493(1997)125<2662:TGOHGT>2.0.CO;2.

Bryan, G. H., and R. Rotunno, 2009: Evaluation of an analytical model for the maximum intensity of tropical cyclones. *J. Atmos. Sci.*, **66**, 3042–3060, doi:10.1175/2009JAS3038.1.

Charney, J. G., and A. Eliassen, 1964: On the growth of the hurricane depression. *J. Atmos. Sci.*, **21**, 68–75, doi:10.1175/1520-0469(1964)021<0068:OTGOTH>2.0.CO;2.

Davis, C. A., 2015: The formation of moist vortices and tropical cyclones in idealized simulations. *J. Atmos. Sci.*, **72**, 3499–3516, doi:10.1175/JAS-D-15-0027.1.

——, and L. F. Bosart, 2001: Numerical simulations of the genesis of Hurricane Diana (1984). Part I: Control simulation. *Mon. Wea. Rev.*, **129**, 1859–1881, doi:10.1175/1520-0493(2001)129<1859:NSOTGO>2.0.CO;2.

——, and D. A. Ahijevych, 2012: Mesoscale structural evolution of three tropical weather systems observed during PREDICT. *J. Atmos. Sci.*, **69**, 1284–1305, doi:10.1175/JAS-D-11-0225.1.

Dunkerton, T. J., M. T. Montgomery, and Z. Wang, 2009: Tropical cyclogenesis in a tropical wave critical layer: Easterly waves. *Atmos. Chem. Phys.*, **9**, 5587–5646, doi:10.5194/acp-9-5587-2009.

Emanuel, K. A., 1989: The finite-amplitude nature of tropical cyclogenesis. *J. Atmos. Sci.*, **46**, 3431–3456, doi:10.1175/1520-0469(1989)046<3431:TFANOT>2.0.CO;2.

——, 1994: *Atmospheric Convection.* 1st ed. Oxford University Press, 592 pp.

——, 1997: Some aspects of hurricane inner-core dynamics and energetics. *J. Atmos. Sci.*, **54**, 1014–1026, doi:10.1175/1520-0469(1997)054<1014:SAOHIC>2.0.CO;2.

Enagonio, J., and M. T. Montgomery, 2001: Tropical cyclogenesis via convectively forced vortex Rossby waves in a shallow water primitive equation model. *J. Atmos. Sci.*, **58**, 685–706, doi:10.1175/1520-0469(2001)058<0685:TCVCFV>2.0.CO;2.

Halperin, D. J., H. E. Fuelberg, R. E. Hart, J. H. Cossuth, P. Sura, and R. J. Pasch, 2013: An evaluation of tropical cyclone genesis forecasts from global numerical models. *Wea. Forecasting*, **28**, 1423–1445, doi:10.1175/WAF-D-13-00008.1.

Hendricks, E. A., M. T. Montgomery, and C. A. Davis, 2004: The role of vortical hot towers in the formation of Tropical Cyclone Diana (1984). *J. Atmos. Sci.*, **61**, 1209–1232, doi:10.1175/1520-0469(2004)061<1209:TROVHT>2.0.CO;2.

Houze, R. A., 1997: Stratiform precipitation in regions of convection: A meteorological paradox? *Bull. Amer. Meteor. Soc.*, **78**, 2179–2196, doi:10.1175/1520-0477(1997)078<2179:SPIROC>2.0.CO;2.

——, 2010: Clouds in tropical cyclones. *Mon. Wea. Rev.*, **138**, 293–344, doi:10.1175/2009MWR2989.1.

Kerns, B. W., and S. S. Chen, 2015: Subsidence warming as an underappreciated ingredient in tropical cyclogenesis. Part I: Aircraft observations. *J. Atmos. Sci.*, **72**, 4237–4260, doi:10.1175/JAS-D-14-0366.1.

Kilroy, G., and R. K. Smith, 2013: A numerical study of rotating convection during tropical cyclogenesis. *Quart. J. Roy. Meteor. Soc.*, **139**, 1255–1269, doi:10.1002/qj.2022.

Komaromi, W. A., 2013: An investigation of composite dropsonde profiles for developing and nondeveloping tropical waves during the 2010 PREDICT field campaign. *J. Atmos. Sci.*, **70**, 542–558, doi:10.1175/JAS-D-12-052.1.

Moller, J. D., and M. T. Montgomery, 2000: Tropical cyclone evolution via potential vorticity anomalies in a three-dimensional balance model. *J. Atmos. Sci.*, **57**, 3366–3387, doi:10.1175/1520-0469(2000)057<3366:TCEVPV>2.0.CO;2.

Montgomery, M. T., and J. Enagonio, 1998: Tropical cyclogenesis via convectively forced vortex Rossby waves in a three-dimensional quasigeostrophic model. *J. Atmos. Sci.*, **55**, 3176–3207, doi:10.1175/1520-0469(1998)055<3176:TCVCFV>2.0.CO;2.

——, M. E. Nicholls, T. A. Cram, and A. B. Saunders, 2006: A vortical hot tower route to tropical cyclogenesis. *J. Atmos. Sci.*, **63**, 355–386, doi:10.1175/JAS3604.1.

——, N. V. Sang, R. K. Smith, and J. Persing, 2009: Do tropical cyclones intensify by WISHE? *Quart. J. Roy. Meteor. Soc.*, **135**, 1697–1714, doi:10.1002/qj.459.

Neelin, J. D., and I. M. Held, 1987: Modeling tropical convergence based on the moist static energy budget. *Mon. Wea. Rev.*, **115**, 3–12, doi:10.1175/1520-0493(1987)115<0003:MTCBOT>2.0.CO;2.

Nguyen, L. T., J. Molinari, and D. Thomas, 2014: Evaluation of tropical cyclone center identification methods in numerical models. *Mon. Wea. Rev.*, **142**, 4326–4339, doi:10.1175/MWR-D-14-00044.1.

Nicholls, M. E., and M. T. Montgomery, 2013: An examination of two pathways to tropical cyclogenesis occurring in idealized simulations with a cloud-resolving numerical model. *Atmos. Chem. Phys.*, **13**, 5999–6022, doi:10.5194/acp-13-5999-2013.

Nolan, D. S., 2007: What is the trigger for tropical cyclogenesis? *Aust. Meteor. Mag.*, **56**, 241–266.

Ooyama, K., 1969: Numerical simulation of the life cycle of tropical cyclones. *J. Atmos. Sci.*, **26**, 3–40, doi:10.1175/1520-0469(1969)026<0003:NSOTLC>2.0.CO;2.

——, 1982: Conceptual evolution of the theory and modeling of the tropical cyclone. *J. Meteor. Soc. Japan*, **60**, 369–379, doi:10.2151/jmsj1965.60.1_369.

Raymond, D. J., 1995: Regulation of moist convection over the west Pacific warm pool. *J. Atmos. Sci.*, **52**, 3945–3959, doi:10.1175/1520-0469(1995)052,3945:ROMCOT.2.0.CO;2.

——, 2012: Balanced thermal structure of an intensifying tropical cyclone. *Tellus*, **64A**, 19 181, doi:10.3402/tellusa.v64i0.19181.

——, and S. L. Sessions, 2007: Evolution of convection during tropical cyclogenesis. *Geophys. Res. Lett.*, **34**, L06811, doi:10.1029/2006GL028607.

——, C. López-Carrillo, and L. López Cavazos, 1998: Case-studies of developing east Pacific easterly waves. *Quart. J. Roy. Meteor. Soc.*, **124**, 2005–2034, doi:10.1002/qj.49712455011.

——, S. L. Sessions, and Ž. Fuchs, 2007: A theory for the spinup of tropical depressions. *Quart. J. Roy. Meteor. Soc.*, **133**, 1743–1754, doi:10.1002/qj.125.

——, ——, A. H. Sobel, and Ž. Fuchs, 2009: The mechanics of gross moist stability. *J. Adv. Model. Earth Syst.*, **1** (9), doi:10.3894/JAMES.2009.1.9.

——, ——, and C. Lopez Carrillo, 2011: Thermodynamics of tropical cyclogenesis in the northwest Pacific. *J. Geophys. Res.*, **116**, D18101, doi:10.1029/2011JD015624.

——, S. Gjorgjievska, S. L. Sessions, and Z. Fuchs, 2014: Tropical cyclogenesis and mid-level vorticity. *Aust. Meteor. Oceanogr. J.*, **64**, 11–25, doi:10.22499/2.6401.003.

Schubert, W. H., and J. J. Hack, 1983: Transformed Eliassen balanced vortex model. *J. Atmos. Sci.*, **40**, 1571–1583, doi:10.1175/1520-0469(1983)040<1571:TEBVM>2.0.CO;2.

Shapiro, L. J., and H. E. Willoughby, 1982: The response of balanced hurricanes to local sources of heat and momentum. *J. Atmos. Sci.*, **39**, 378–394, doi:10.1175/1520-0469(1982)039<0378:TROBHT>2.0.CO;2.

Simpson, J., E. Ritchie, G. J. Holland, J. Halverson, and S. Stewart, 1997: Mesoscale interactions in tropical cyclone genesis. *Mon. Wea. Rev.*, **125**, 2643–2661, doi:10.1175/1520-0493(1997)125<2643:MIITCG>2.0.CO;2.

Smith, R. K., M. T. Montgomery, and N. Van Sang, 2009: Tropical cyclone spin-up revisited. *Quart. J. Roy. Meteor. Soc.*, **135**, 1321–1335, doi:10.1002/qj.428.

Tang, B. H., 2017: Coupled dynamic–thermodynamic forcings during tropical cyclogenesis. Part II: Axisymmetric experiments. *J. Atmos. Sci.*, **74**, 2279–2291, doi:10.1175/JAS-D-17-0049.1.

——, and K. Emanuel, 2012: Sensitivity of tropical cyclone intensity to ventilation in an axisymmetric model. *J. Atmos. Sci.*, **69**, 2394–2413, doi:10.1175/JAS-D-11-0232.1.

Wang, Z., 2012: Thermodynamic aspects of tropical cyclone formation. *J. Atmos. Sci.*, **69**, 2433–2451, doi:10.1175/JAS-D-11-0298.1.

——, 2014: Role of cumulus congestus in tropical cyclone formation in a high-resolution numerical model simulation. *J. Atmos. Sci.*, **71**, 1681–1700, doi:10.1175/JAS-D-13-0257.1.

Willoughby, H. E., 1979: Forced secondary circulations in hurricanes. *J. Geophys. Res.*, **84**, 3173–3183, doi:10.1029/JC084iC06p03173.

Zawislak, J., and E. J. Zipser, 2014: Analysis of the thermodynamic properties of developing and nondeveloping tropical disturbances using a comprehensive dropsonde dataset. *Mon. Wea. Rev.*, **142**, 1250–1264, doi:10.1175/MWR-D-13-00253.1.

Zhang, D.-L., and L. Zhu, 2012: Roles of upper-level processes in tropical cyclogenesis. *Geophys. Res. Lett.*, **39**, L17804, doi:10.1029/2012GL053140.